IOP Publishing New J. Phys. 24 (2022) 123015 https://doi.org/10.1088/1367-2630/aca81e

New Journal of Physics
The open access journal at the forefront of physics

Deutsche Physikalische Gesellschaft DPG
IOP Institute of Physics

Published in partnership with: Deutsche Physikalische Gesellschaft and the Institute of Physics

OPEN ACCESS

RECEIVED
27 July 2022

REVISED
26 October 2022

ACCEPTED FOR PUBLICATION
2 December 2022

PUBLISHED
15 December 2022

PAPER

Heat transport in an optical lattice via Markovian feedback control

Ling-Na Wu* and **André Eckardt**

Institut für Theoretische Physik, Technische Universität Berlin, Hardenbergstraße 36, Berlin 10623, Germany
* Author to whom any correspondence should be addressed.

E-mail: lingna.wu@tu-berlin.de

Keywords: Markovian feedback control, Bose–Hubbard model, heat transport, master equation, kinetic theory, Monte-Carlo simulation

Abstract

Ultracold atoms offer a unique opportunity to study many-body physics in a clean and well-controlled environment. However, the isolated nature of quantum gases makes it difficult to study transport properties of the system, which are among the key observables in condensed matter physics. In this work, we employ Markovian feedback control to synthesize two effective thermal baths that couple to the boundaries of a one-dimensional Bose–Hubbard chain. This allows for the realization of a heat-current-carrying state. We investigate the steady-state heat current, including its scaling with system size and its response to disorder. In order to study large systems, we use semi-classical Monte-Carlo simulation and kinetic theory. The numerical results from both approaches show, as expected, that for non- and weakly interacting systems with and without disorder one finds the same scaling of the heat current with respect to the system size as it is found for systems coupled to thermal baths. Finally, we propose and test a scheme for measuring the energy flow. Thus, we provide a route for the quantum simulation of heat-current-carrying steady states of matter in atomic quantum gases.

1. Introduction

Ultracold atoms are well isolated from their environment and free of impurities or disorder, unless these properties are engineered on purpose in a controlled fashion. Moreover, they are highly tunable and can be manipulated and probed on their (large) intrinsic time and length scales. These properties make quantum gases a unique platform for quantum simulation of condensed matter models [1]. The measurement of transport constitutes a key element in the toolbox. Transport plays a crucial role in understanding states of matter in and out of equilibrium [2, 3]. The study of transport properties in real materials is always influenced by the effect of impurities, lattice defects and phonons. Ultracold atoms, in turn, offer to study transport under extremely clean and flexible conditions. However, the isolated nature of quantum gases prevents a direct connection of the system, e.g. to leads or extended thermal baths of different temperature.

In order to investigate the transport properties of quantum gases, a variety of approaches have been exploited. For instance, particle transport has been investigated by observing the response of the system to variations of the external potential via measuring the density distribution [4, 5], the quasimomentum distribution [6, 7], monitoring the center of mass motion [8–11], and expansion dynamics [12–22], or by studying mass flow through optically structured mesoscopic devices [23–26]. Spin transport was studied by introducing spin inhomogeneities followed by monitoring the spin evolution [27–30] or investigating the decoherence of spin texture [31–36]. And heat transport was investigated by locally heating the system, after which the equilibration is studied by monitoring the temperature bias [37] or particle imbalance [38, 39]. However, in all these experiments, transport occurs as a transient phenomenon only.

In this work, we employ Markovian feedback control [40] to engineer two effective thermal baths that are coupled to a one-dimensional Bose–Hubbard chain. This allows for the realization of a heat-current-carrying steady state. As a measurement-based approach, Markovian feedback control continuously adds a signal-proportional feedback term to the system Hamiltonian. The dynamics of the system is then described by a feedback-modified Lindblad master equation (ME) [40]. By properly choosing the measurement and

feedback operators, the system dynamics can be steered towards a desired target state. The Markovian feedback method has been applied to various control problems, including the stabilization of arbitrary one-qubit quantum states [41, 42], the manipulation of quantum entanglement between two qubits [43–46] as well as optical and spin squeezing [47–49]. In our previous works, we have shown that Markovian feedback control can be used to cool a bosonic quantum gas in an optical lattice [50] and to engineer a thermal bath [51]. Here, we will generalize such a feedback scheme to engineer two thermal baths at the boundaries of an optical lattice and study the heat transport through the chain induced by it. Different from our previous works [50, 51], this requires to work out a scheme for engineering artificial thermal baths by employing local measurements and feedback on a few lattice sites only.

The focus of this work is quantum engineering of heat-current-carrying state. To benchmark our scheme, we study the scaling behavior of heat current. But the transport behavior itself is not our focus. We study the scaling behavior for noninteracting cases and also interacting cases with fixed particles. The exponentially increasing Hilbert space dimension with system size does not allow us to study the scaling behavior for interacting cases with fixed filling factor. While our scheme opens the opportunity to investigate this question experimentally in a quantum simulation, where heat-current-carrying states also of larger interacting systems are prepared using feedback control.

The paper is organized as follows: in section 2, we introduce our model and some basics of Markovian feedback control. This is followed by the description of a two-site feedback scheme in section 3, which can be used to engineer a finite-temperature bath. In section 4, we present a scheme which allows for the realization of a heat-current-carrying state. We study the steady-state heat current of the system, including its scaling behavior with system size (see section 4.3) and its response to disorder (see section 4.4), and compare the results to those when the system is coupled to real thermal baths. The experimental implementation of our scheme is discussed in section 5, including the measurement of heat current by measuring single-particle density matrix. A summary of the main results is presented in section 6 to conclude.

2. Model and Markovian feedback scheme

The system under consideration is a one-dimensional optical lattice with N interacting bosonic atoms, which can be described by the Bose–Hubbard model,

$$H=-J\sum_{l=1}^{M-1}(a_l^\dagger a_{l+1}+a_{l+1}^\dagger a_l)+\frac{U}{2}\sum_{l=1}^{M}n_l(n_l-1)+\sum_{l=1}^{M}V_l n_l, \tag{1}$$

where a_l annihilates a particle on site l and $n_l=a_l^\dagger a_l$ counts the particle number on site l, with $\sum_l n_l=N$. The first term in (1) describes tunneling between neighboring sites with rate J, the second term denotes on-site interactions with strength U and the last term describes an on-site potential. In the following discussion, $V_l=0$ unless stated otherwise.

Let us consider a homodyne measurement of an operator c. The dynamical evolution of the system is then described by the stochastic ME (SME) [52] ($\hbar=1$ hereafter),

$$d\rho_c=-i[H,\rho_c]dt+\mathcal{D}[c]\rho_c dt+\mathcal{H}[c]\rho_c dW,$$

with $\mathcal{H}[c]\rho:=c\rho+\rho c^\dagger-\mathrm{Tr}[(c+c^\dagger)\rho]\rho$ and $\mathcal{D}[c]\rho:=c\rho c^\dagger-\frac{1}{2}(c^\dagger c\rho+\rho c^\dagger c)$. Here ρ_c denotes the density matrix of the system conditioned on the measurement result,

$$I_{\mathrm{hom}}=\mathrm{Tr}[(c+c^\dagger)\rho_c]+\xi(t)=\langle c+c^\dagger\rangle_c+\xi(t).$$

The first term in I_{hom} denotes the mean value of the instantaneous quadrature of the output field from the homodyne measurement, and the second term describes Gaussian white noise with $\xi(t)=dW/dt$ and dW being the standard Wiener increment with mean zero and variance dt. The quantum backaction of a weak measurement can be used for tailoring the system's dynamics and to prepare target states. While the state generated in this way is conditional due to the nondeterministic nature of measurement, the introduction of feedback using the information acquired from the measurements allows to steer the system's dynamics into a desired state.

Here we consider a direct feedback strategy, where a signal-dependent, i.e. conditional, feedback term $I_{\mathrm{hom}}F$ is added to the Hamiltonian. The effect of feedback is then described by

$$[\dot{\rho}_c(t)]_{\mathrm{fb}}=-iI_{\mathrm{hom}}[F,\rho_c]\equiv I_{\mathrm{hom}}\mathcal{K}\rho_c.$$

By expanding the feedback superoperator $\exp[\mathcal{K}I_{\rm hom}dt]$ to second order, we obtain

$$\rho_c(t+dt) = \{1+\mathcal{K}(\langle c+c^\dagger\rangle_c dt + dW) + \mathcal{K}^2 dt/2\}\{1+\mathcal{H}[-iH]dt + \mathcal{D}[c]dt + \mathcal{H}[c]dW\}\rho_c(t),$$

where we have used $dW^2 = dt$. Keeping terms up to first order in dt, we arrive at the feedback-modified SME [40, 52]

$$d\rho_c = -i[H+H_{\rm fb},\rho_c]dt + \mathcal{D}[A]\rho_c dt + \mathcal{H}[A]\rho_c dW,$$

with operators

$$A = c - iF, \quad H_{\rm fb} = \frac{1}{2}(c^\dagger F + Fc). \tag{2}$$

By taking the ensemble average of the possible measurement outcomes, we arrive at the feedback-modified ME [40]

$$\dot\rho = -i[H+H_{\rm fb},\rho] + \mathcal{D}[A]\rho. \tag{3}$$

The effect induced by the feedback loop is seen to replace the collapse operator c by A and to add an extra term $H_{\rm fb}$ to the Hamiltonian. The latter is proportional to measurement strength and thus can be safely neglected for weak measurements.

3. Two-site feedback scheme

Before approaching the scenario relevant for heat transport, where the feedback is mimicking two thermal baths of different temperature at both ends of the system, let us first investigate how the *local* coupling to a single bath can be realized. Previously, we considered already the engineering of a thermal bath using measurement and feedback operators acting globally on all sites of a lattice [51]. In contrast, we now consider the following two-site measurement and feedback operator

$$c_l = \sqrt{\gamma}(x_l n_l - x_l^{-1} n_{l+1}), \quad \lambda F_l = -i\lambda\sqrt{\gamma}(a_l^\dagger a_{l+1} - a_{l+1}^\dagger a_l), \tag{4}$$

where γ is the measurement strength, λ is a free parameter to be determined, $x_l = g_{l+1}/g_l$ and g_l are the coefficients of the single-particle ground state, i.e. $|g\rangle = \sum_l g_l|l\rangle$. The feedback-modified collapse operator then reads

$$A_l = c_l - i\lambda F_l. \tag{5}$$

Note that the sites l and $l+1$ where to perform the measurement and feedback can be any neighboring two sites on the lattice.

For N non-interacting particles, with $\lambda = 1$, one can show that $A_l|g\rangle^{\otimes N} = 0$, where $|g\rangle^{\otimes N}$ denotes the ground state of the system, with all particles occupying the single-particle ground state, $|g\rangle$. It is easy to check it for the single-particle problem, where the collapse operator reduces to

$$A_l = \frac{g_{l+1}}{g_l}|l\rangle\langle l| - \frac{g_l}{g_{l+1}}|l+1\rangle\langle l+1| - (|l\rangle\langle l+1| - |l+1\rangle\langle l|).$$

Applying it to the ground state $|g\rangle$, one gets

$$A_l|g\rangle = g_{l+1}|l\rangle - g_l|l+1\rangle - g_{l+1}|l\rangle + g_l|l+1\rangle = 0.$$

When there are no interactions between the particles, the multi-particle problem is equivalent to the single-particle problem. Namely, the ground state of the system is a dark state of the collapse operator A_l. Assuming weak measurements with strength $\gamma \ll J$, where the impact of the additional term in the Hamiltonian $H_{\rm bf} \propto \gamma$ is negligible, the dissipative dynamics will then drive the system towards the ground state (if it is the unique dark state of the collapse operator).

In figure 1, we show the fidelity between the steady state of the ME (3) for our two-site feedback scheme (4), $\rho_{\rm ss}$, and the ground state of the system (1), $|G\rangle$, i.e.

$$f = \sqrt{\langle G|\rho_{\rm ss}|G\rangle}, \tag{6}$$

as a function of the measurement strength γ for two different lattice sizes with $N = 2$ non-interacting particles: (a) $M = 7$ and (b) $M = 8$. Different colored curves correspond to schemes performing at different

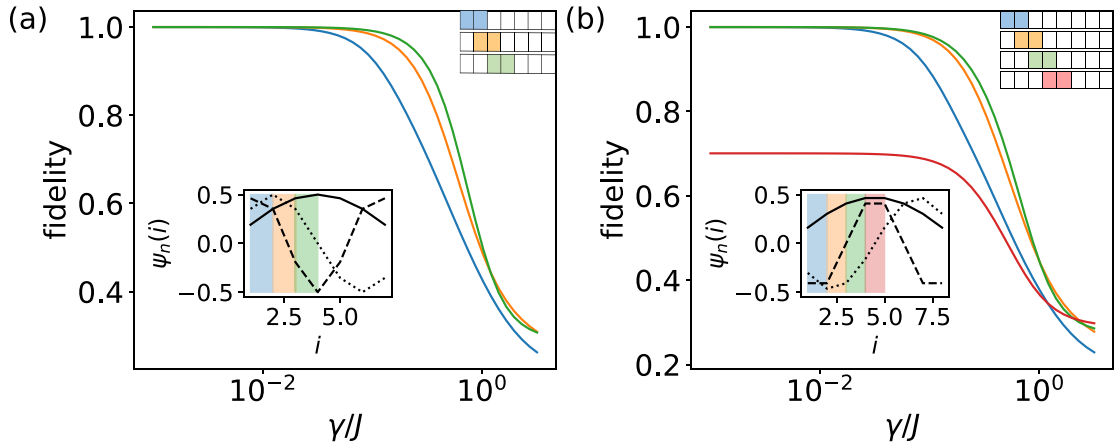

Figure 1. The fidelity (6) between the steady state of the ME (3) for our two-site feedback scheme (4) and the ground state of the system (1) as a function of the measurement strength γ for two different lattice sizes with $N = 2$ non-interacting particles: (a) $M = 7$ and (b) $M = 8$. Different colored curves correspond to schemes performing at different sites as indicated by the sketch at the upper right corner with the corresponding colors. As expected, for weak measurements $\gamma \ll J$, the fidelity approaches 1. The only case where the feedback-controlled system does not settle down to the ground state (see the red curve in (b)) for weak measurements is due to the fact that the ground state is not the unique dark state of the collapse operator. From the inset, which shows the first three eigenstates of the system, one can see that the first excited state for $M = 8$ in (b) as denoted by the dashed line has the same wavefunction values as the ground state (see solid line) at the feedback-controlled sites (site 4 and site 5), and thus is also a dark state of the collapse operator.

sites as indicated by the sketch at the upper right corner with the corresponding colors. As expected, for weak measurements $\gamma \ll J$, the fidelity approaches 1. The only case where the feedback-controlled system does not settle down to the ground state (see the red curve in (b)) for weak measurements is due to the fact that the ground state is not the unique dark state of the collapse operator. Namely, from the inset, which shows the first three eigenstates of the system, one can see that the first excited state for $M = 8$ in (b) as denoted by the dashed line has the same wavefunction values as the ground state (see solid line) at the feedback-controlled sites (site 4 and site 5), and thus is also a dark state of the collapse operator.

For $0 < \lambda < 1$, the proposed scheme can be used to engineer a finite-temperature bath. In figure 2, we show the effective temperature of the feedback-synthesized bath as a function of the feedback strength λ for (a) non-interacting and (c) interacting systems. The effective temperature is fixed by fitting the distribution of the steady state in the eigenbasis to a thermal distribution with temperature being the fitting parameter. The inset shows the fidelity between the steady state and the corresponding effective thermal state, which is close to 1 over the whole parameter regime. As a second measure, we compare the probability distribution in the eigenstate basis for the steady states at various λ (solid lines) marked in figures 2(a), (c) to the corresponding thermal states (dashed lines) in figures 2(b), (d). They are found to agree with each other very well.

4. Heat transport

4.1. Model

We use the two-site feedback scheme to heat up the system on one side and cool it down on the other side, see the sketch in figure 3. Note that for the following discussion, we stick to the scenario that the left lead is located on site one and two, while the right lead is located on site $M-2$ and $M-1$. The asymmetric arrangement on feedback-controlled sites for the two baths is to avoid the otherwise result that the system will be effectively coupled to one thermal bath at the average temperature of the two synthesized baths [53]. The two measurement operations are assumed to be independent of each other (see section 5 for the experimental implementation), giving rise to uncorrelated signals. The dynamics of the system is described by the feedback ME,

$$\dot{\rho} = \mathcal{L}\rho = -i[H,\rho] + \mathcal{L}_L\rho + \mathcal{L}_R\rho, \tag{7}$$

where

$$\mathcal{L}_\mu\rho = -i[H^\mu_{\rm fb},\rho] + \mathcal{D}[A_\mu](\rho), \quad (\mu = L,R) \tag{8}$$

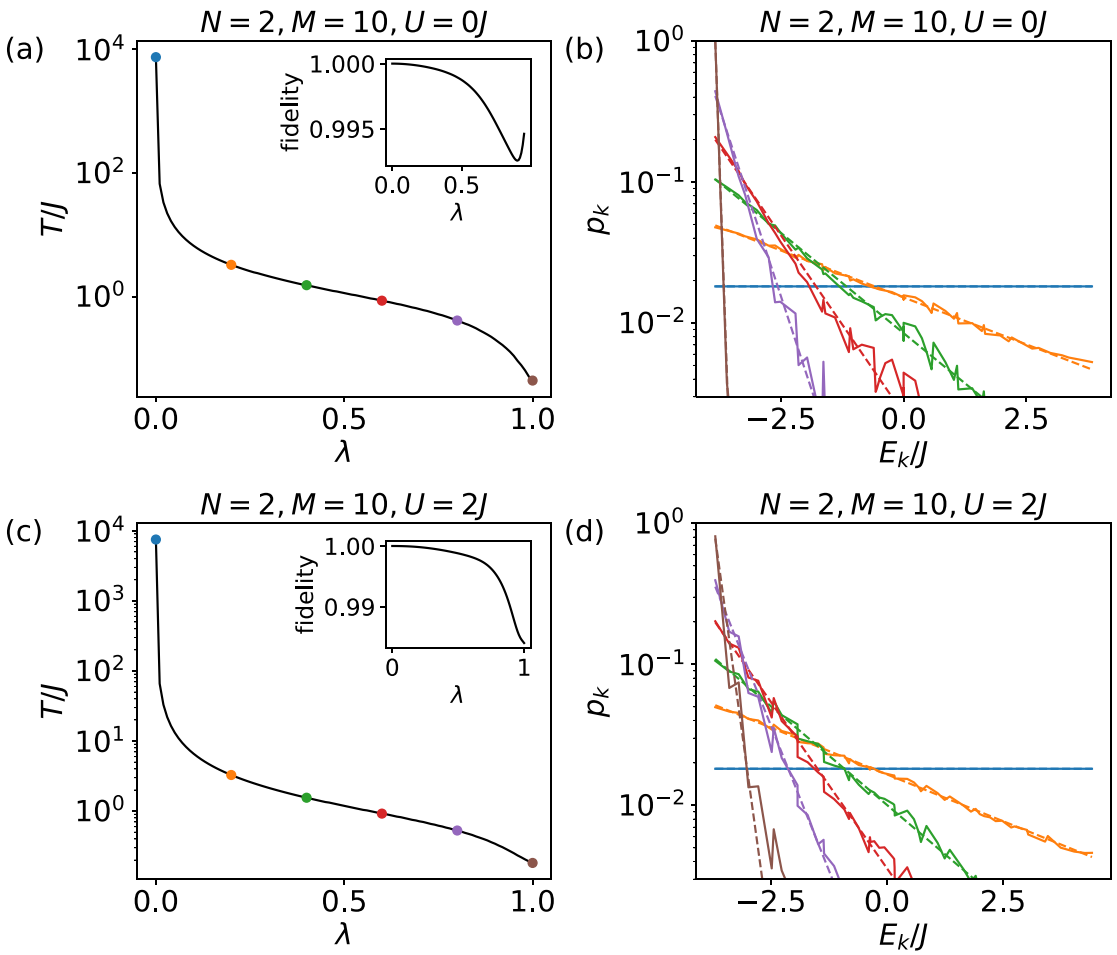

Figure 2. Engineering a finite-temperature bath using two-site feedback scheme (4). (a), (c) The effective temperature of the feedback-synthesized bath as a function of the feedback strength λ. The effective temperature is fixed by fitting the distribution of the steady state in the eigenbasis to a thermal distribution with temperature being the fitting parameter. The inset shows the fidelity between the steady state and the corresponding effective thermal state. (b), (d) The distribution of the steady state on the eigenbasis for various λ marked in (a), (c). k is the label of the kth eigenstate, with energy in ascending order. Dashed lines are the corresponding thermal distributions. Parameters are $V_l = 0$, $\gamma = 0.01J$.

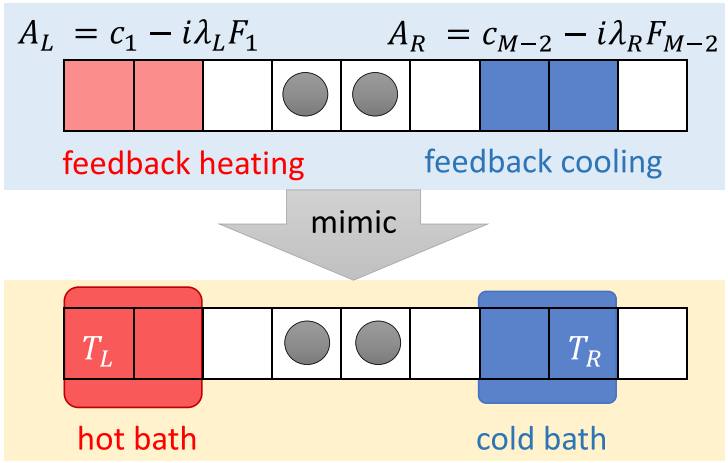

Figure 3. A sketch of our feedback scheme for realizing a heat-current-carrying state. A one-dimensional optical lattice is cooled and heated at both ends via feedback control, as shown in the upper panel in blue background. This mimics the effect of coupling the system locally to a hot bath and a cold bath (see lower panel in yellow background), and thus allows us to study the heat transport property of the system.

describes the impact of the feedback control on the μ side of the chain with $H_{\rm fb}^{L}\equiv H_{\rm fb}^{(1)}$, $H_{\rm fb}^{R}\equiv H_{\rm fb}^{(M-2)}$, $H_{\rm fb}^{(l)}=(c_lF_l+F_lc_l)/2$ and

$$A_L\equiv A_1=c_1-i\lambda_L F_1,\quad A_R\equiv A_{M-2}=c_{M-2}-i\lambda_R F_{M-2}. \tag{9}$$

Cooling is realized by setting $\lambda=1$, corresponding to a zero-temperature bath, and heating by setting $0<\lambda<1$, corresponding to finite positive temperatures.

4.2. Heat current

The feedback control induces quantum jumps between the eigenstates of the system, and thus changes the energy of the system. Take feedback cooling (to the ground state) as an example, starting from an arbitrary initial state (and thus an arbitrary initial energy), the feedback control will drive the system towards the ground state, which possesses the lowest energy. The energy of the system thus changes with time until the system relaxes to the steady state. By feedback heating the system up on one end, and cooling it down on the other end, one can then induce an energy transfer across the chain, realizing a heat-current-carrying steady state.

The heat current $\mathcal{J}$ is calculated from the continuity equation for energy,

$$\frac{d\langle H\rangle}{dt}=\mathcal{J}_L+\mathcal{J}_R. \tag{10}$$

It follows from the ME (7) that

$$\frac{d\langle H\rangle}{dt}={\rm Tr}\left\{H\mathcal{L}_L\rho\right\}+{\rm Tr}\left\{H\mathcal{L}_R\rho\right\}.$$

So we have

$$\mathcal{J}_L={\rm Tr}\left\{H\mathcal{L}_L\rho\right\},\quad \mathcal{J}_R={\rm Tr}\left\{H\mathcal{L}_R\rho\right\}. \tag{11}$$

In the steady state, $d\langle H\rangle/dt=0$. Thus, the steady-state heat current is

$$\mathcal{J}_{\rm ss}=\mathcal{J}_L=-\mathcal{J}_R={\rm Tr}\left\{H\mathcal{L}_L\rho_{\rm ss}\right\}=-{\rm Tr}\left\{H\mathcal{L}_R\rho_{\rm ss}\right\}. \tag{12}$$

Note that there is no particle current in the system. The feedback control conserves particle number. Also in the thermal bath case, the coupling to thermal baths only induces quantum jumps between the eigenstates of the system, and does not change the particle number in the system.

Figure 4 shows the steady-state heat current of a system with $N=1$ particle in a lattice with $M=10$ sites as a function of the feedback strength λ_L (see (a) and (b)) and the effective temperature T_L (see (c) and (d)) of the left bath [1]. For the right bath, in (a, c) $\lambda_R=1$, which corresponds to a zero-temperature bath ($T_R=0$); in (b, d) $\lambda_R=0$, which corresponds to an infinite-temperature bath ($T_R=\infty$). As expected, the heat current in both cases increases with the temperature imbalance between the two baths. Similar behavior is observed when the system is coupled to real thermal baths [2], as shown in figures 4(e), (f). It is not expected that an exact mapping of heat current exists between our feedback scheme and the real thermal bath case. For the latter, heat current depends not only on the temperature of the baths, but also on the bath correlation function (e.g., spectral density), which has no correspondence in our scheme. In the following discussion, we will focus on the case with $\lambda_R=1$ for our scheme.

4.3. System-size scaling

We are interested in the scaling of the steady-state heat current with system size. To study this property, we have to deal with large systems, which are not accessible by exact diagonalization (ED). For a system with N particles and M sites, the dimension of the Hilbert space is $D=(N+M-1)!/N!/(M-1)!$, which means the Liouvillian superoperator $\mathcal{L}$ is a D^2 by D^2 matrix. For instance, for $M=4$ and $N=8$, $D=330$, the Liouvillian superoperator will be a 108 900 by 108 900 matrix. This simple example shows that it is hard to treat large systems by using the ED approach. In order to circumvent this problem, we resort to two different approaches: kinetic theory and semi-classical Monte Carlo (MC) simulation, as described in the following.

[1] The single-particle problem can be solved analytically, see appendix A.

[2] See appendix B for the calculation of heat transport when the system is coupled to thermal baths.

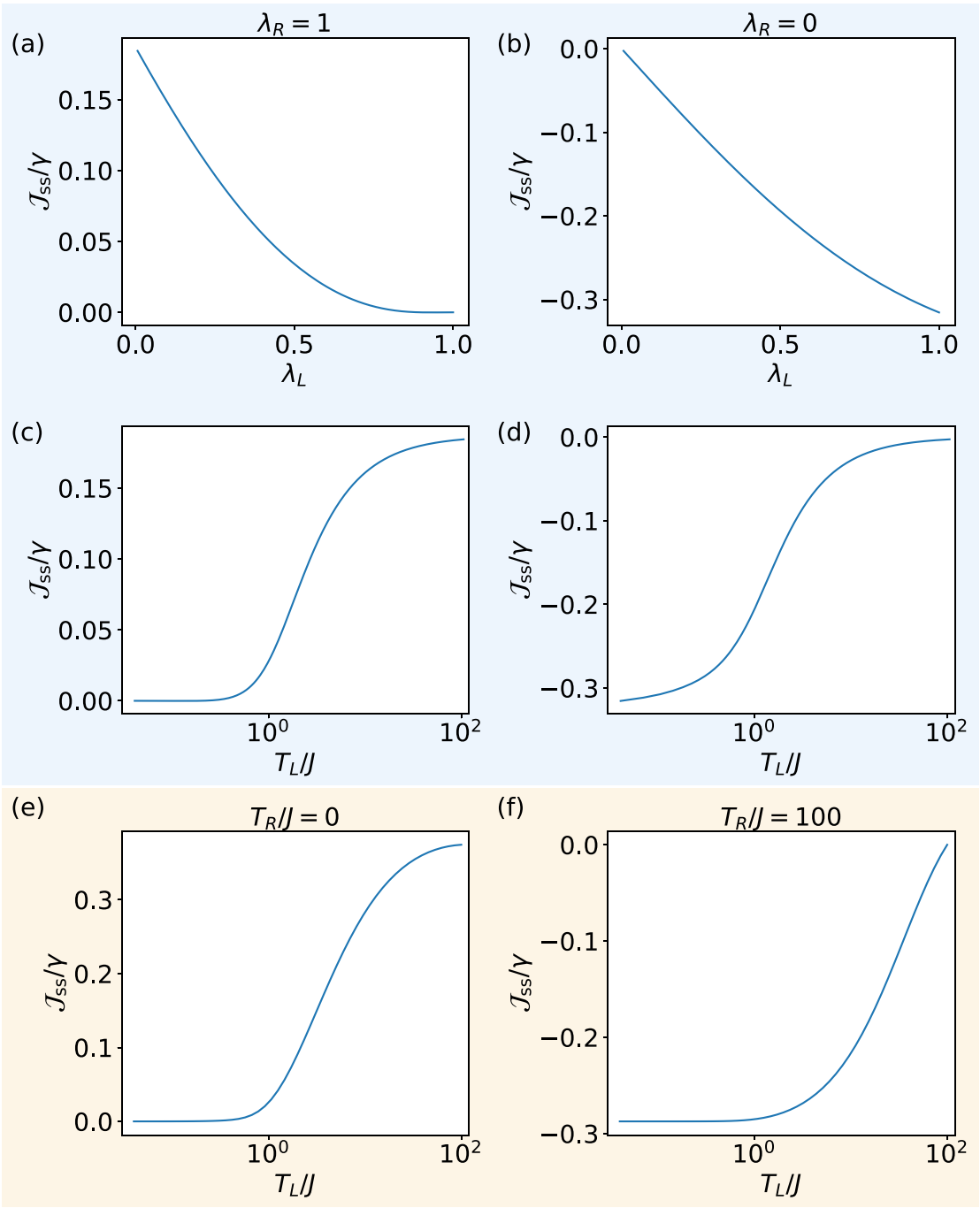

Figure 4. The panels in blue background (a)–(d) are the results for our scheme. The steady-state heat current is shown as a function of (a), (b) the feedback strength λ_L and (c), (d) the effective temperature T_L of the left bath. For the right bath, (a), (c) $\lambda_R = 1$, which corresponds to a zero-temperature bath; (b), (d) $\lambda_R = 0$, which corresponds to an infinite-temperature bath. In both cases, the heat current increases with the temperature imbalance between the two baths. Similar behavior is observed when the system is coupled to real thermal bath, as shown in the panels (e), (f) in yellow background. Parameters are $N = 1, M = 10, V_l = 0, \gamma = 0.01J$.

For the non-interacting case, the system Hamiltonian reads

$$H = \sum_k \epsilon_k n_k,$$

with single-particle eigenenergy $\epsilon_k = -2J\cos\frac{k\pi}{M+1}$ in the absence of on-site potential. Here $n_k = c_k^\dagger c_k$ counts the number of particles in the single-particle eigenstate $|k\rangle$, with $c_k^\dagger = \sum_l \langle l|k\rangle a_l^\dagger$ being the corresponding creation operator. The continuity equation for energy then reads

$$\frac{d\langle H\rangle}{dt} = \sum\nolimits_k \epsilon_k \langle \dot{n}_k\rangle. \tag{13}$$

It depends on the time evolution of the mean occupations $\langle n_k\rangle$, which is governed by

$$\langle \dot{n}_k\rangle = \sum\nolimits_q \left[R_{kq}\langle n_q(1+n_k)\rangle - R_{qk}\langle n_k(1+n_q)\rangle\right], \tag{14}$$

with $R_{kq} = R^L_{kq} + R^R_{kq} = |\langle k|A_L|q\rangle|^2 + |\langle k|A_R|q\rangle|^2$ being the single-particle transfer rate from single-particle eigenstate q to k. The steady-state heat current is given by

$$\mathcal{J}_{\rm ss} = \mathcal{J}_L = \sum\nolimits_k \epsilon_k\langle \dot{n}_k\rangle_L = -\mathcal{J}_R = -\sum\nolimits_k \epsilon_k\langle \dot{n}_k\rangle_R \tag{15}$$

with

$$\langle \dot{n}_k\rangle_\mu = \sum\nolimits_q \left[R^\mu_{kq}\langle n_q(1+n_k)\rangle_{\rm ss} - R^\mu_{qk}\langle n_k(1+n_q)\rangle_{\rm ss}\right], \quad (\mu = L,R). \tag{16}$$

Here the subscript 'ss' of the expectation values denotes the steady-state expectation values, which satisfy

$$\sum\nolimits_q \left[R_{kq}\langle n_q(1+n_k)\rangle_{\rm ss} - R_{qk}\langle n_k(1+n_q)\rangle_{\rm ss}\right] = 0. \tag{17}$$

From the above expression, one can see that even for noninteracting particles, finding the steady state is a true many-body problem due to the interaction of the system with environment. In the following, we describe two approaches to calculate the steady-state expectation values approximately.

4.3.1. Semi-classical MC simulation

In the semi-classical MC simulation [53], the density matrix is approximated by a mixed superposition of Fock states with respect to single-particle eigenstates $\rho = \sum_{\mathbf{n}} p_{\mathbf{n}}|\mathbf{n}\rangle\langle\mathbf{n}|$, with $\mathbf{n} = (n_1, n_2, \ldots, n_M)$, i.e. the off-diagonal elements which decouple with the diagonal elements and decay with time are neglected for weak system-bath coupling [54]. The equations of motion for the Fock-space occupation probabilities $p_{\mathbf{n}}$ are then mapped to a random walk in the classical space spanned by the Fock states $|\mathbf{n}\rangle$ (but not their superpositions). We perform these simulations by using the Gillespie-type algorithm described in [53]. By averaging over the long-time dynamics of many trajectories, we can then compute steady-state expectation values, $\langle n_k\rangle_{\rm ss}, \langle n_k n_q\rangle_{\rm ss}$, etc. The steady-state heat current is then calculated by using equation (15). This approach gives accurate results after sufficient statistical sampling. For a given accuracy, the sampling size increases with increasing system sizes.

4.3.2. Kinetic theory

We use kinetic theory to treat large systems where the semi-classical MC simulation is computationally expensive. The set of equation (14) is not closed as the single-particle correlations depend on two-particle correlations, which in turn depend on three-particle correlations, and so on. To get a closed set of equations, we employ the mean-field approximation $\langle n_k n_q\rangle \approx \langle n_k\rangle\langle n_q\rangle$, which then leads to

$$\langle \dot{n}_k\rangle \approx \sum\nolimits_q \left\{R_{kq}\langle n_q\rangle[1+\langle n_k\rangle] - R_{qk}\langle n_k\rangle[1+\langle n_q\rangle]\right\}.$$

The steady-state heat current is calculated approximately by using equation (15) with

$$\langle \dot{n}_k\rangle_L \approx \sum_q \left\{R^L_{kq}\langle n_q\rangle_{\rm ss}[1+\langle n_k\rangle_{\rm ss}] - R^L_{qk}\langle n_k\rangle_{\rm ss}[1+\langle n_q\rangle_{\rm ss}]\right\}, \tag{18}$$

where the steady-state expectation values are obtained by solving $\langle \dot{n}_k\rangle = 0$, i.e.

$$\sum_q \left\{R_{kq}\langle n_q\rangle_{\rm ss}[1+\langle n_k\rangle_{\rm ss}] - R_{qk}\langle n_k\rangle_{\rm ss}[1+\langle n_q\rangle_{\rm ss}]\right\} = 0. \tag{19}$$

4.3.3. Results

Figure 5 shows the system-size dependence of the steady-state heat current. Let us first focus on the non-interacting case, as shown by the blue data. For a fixed particle number $N = 2$ (see figure 5(a)), the results from the three approaches, i.e. ED (squares), MC simulation (bullets), and mean-field approximation (solid lines), agree with each other. The steady-state heat current is found to decrease with the lattice size M as M^{-1}. For a fixed filling factor at $N/M = 1/5$ (see figure 5(b)), a slight deviation is found between the mean-field results and the MC results. Nevertheless, the results from both approaches show that in this case the current first decreases with system size, but then saturates to a finite value, independent of the

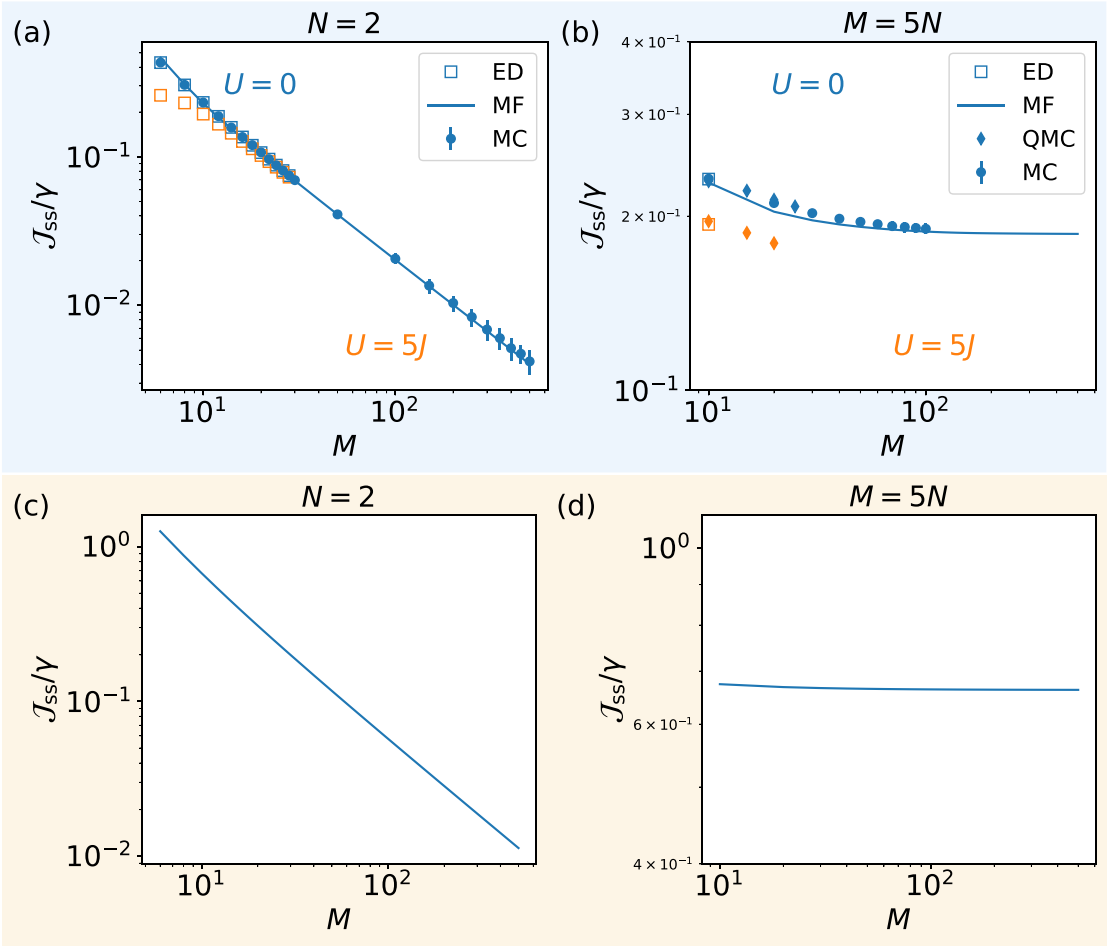

Figure 5. System-size scaling of the steady-state heat current for (a), (c) a fixed particle number $N = 2$ and (b), (d) a fixed filling factor $n = N/M = 1/5$. The panels in blue background (a), (b) are the results for our scheme. The panels in yellow background (c), (d) are the results when the system is coupled to thermal baths. The blue (orange) data denote the results for the non-interacting (interacting) case. The squares denote the results from exact diagonalization (ED). The diamonds denote the results from quantum jump Monte-Carlo simulations (QMCs). The bullets denote the results from semi-classical Monte Carlo (MC) simulation. The solid lines are the results from kinetic theory with mean-field (MF) approximation. For the MC simulation, the results are obtained by averaging over the long-time (up to $\gamma t = 10^5$ for (a) and $\gamma t = 10^6$ for (b)) dynamics of 100 trajectories. The error bar denotes one standard deviation. Parameters are $V_l = 0$, $\gamma = 0.01J$, $\lambda_L = 0.2$, $\lambda_R = 1$, $T_L = 10J$, $T_R = 0.01J$.

lattice size M, corresponding to ballistic transport [3]. These results are consistent with that when the system is coupled to two thermal baths on its ends, as shown in figures 5(c) and (d).

One can understand these scaling behaviors from the expression for the heat current (15) and (16). The single-particle transition rate R^{μ}_{kq} [see equation (A.2) in appendix A] scales with system size M as M^{-2}, and the number of transitions scales as M^2 since the eigenstates (which are coupled by the bath) are delocalized and thus all (M) of them (constituting M^2 pairs) participate in the transition. The scaling of these two factors cancel each other, and thus the scaling of the current is determined by the density-related term $\langle n_q(1+n_k)\rangle$. For a fixed particle number, $\langle n_q(1+n_k)\rangle$ is dominated by the first-order term (density), which scales with the system size as M^{-1}. Hence, the heat current decays with system size as M^{-1}. For a fixed filling factor, $\langle n_q(1+n_k)\rangle$ does not change with system size, and thus the heat current exhibits ballistic behavior, i.e. does not depend on system size.

Now let us turn on interactions. For a fixed particle number, which can be calculated by using ED (the orange squares in figure 5(a)), the interactions are found to have some impact on the steady-state heat current for small systems. While this effect becomes weaker with increasing system sizes, and thus does not change the scaling of the current with system size. For a fixed filling factor, the numerical simulation is challenging. We resort to quantum jump MC method [55, 56], which offers an efficient stochastic simulation of the ME by means of quantum trajectories. We are able to calculate the heat current of the interacting system for up to 20 lattice sites (see orange diamonds in figure 5(b)). We can clearly observe that it is reduced with respect to the heat current for the non-interacting system. Moreover, we can see that it drops with M. The accessible system sizes of 20 do, however, not allow to reach the regime, where the ballistic transport of

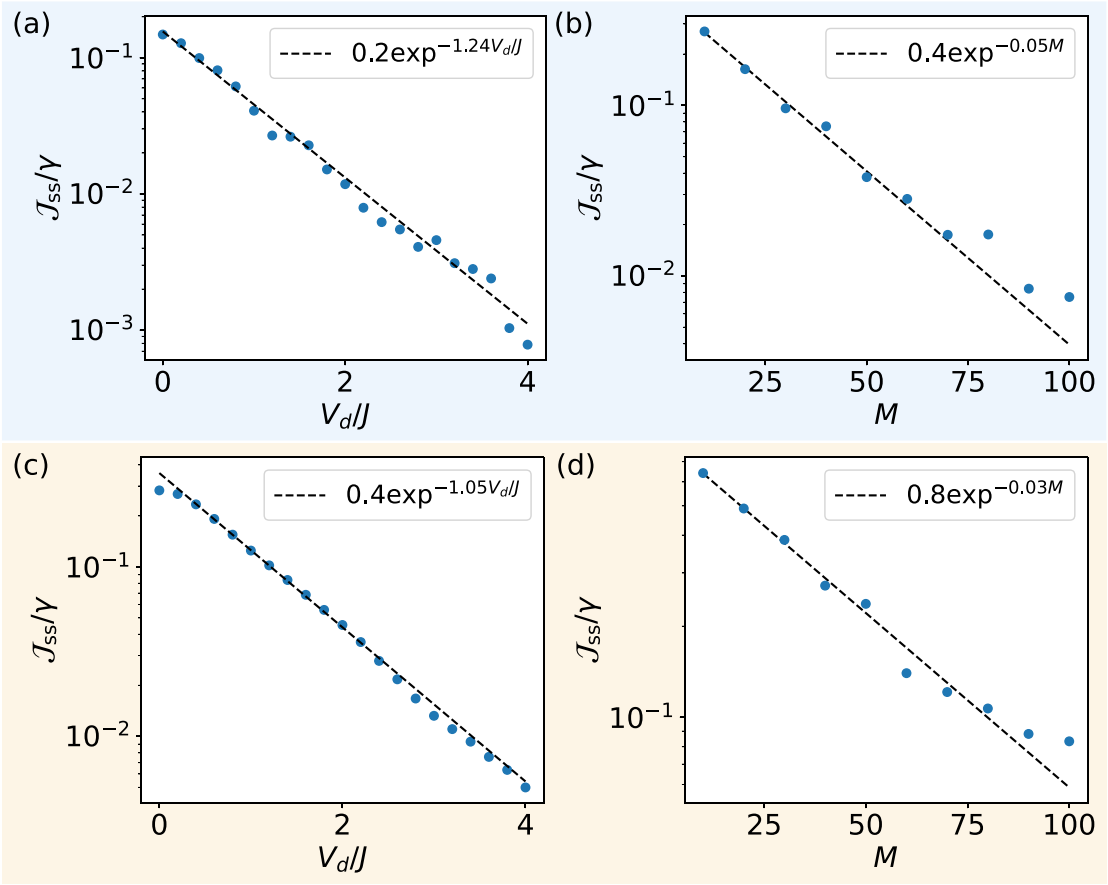

Figure 6. (a), (c) The steady-state heat current $\mathcal{J}_{ss}$ as a function of the disorder strength for one particle on $M = 10$ sites. The results are obtained from exact diagonalization. (b), (d) The system-size scaling of $\mathcal{J}_{ss}$ at $V_d = 0.2J$ for $N = M/5$. The results are obtained from kinetic theory with mean-field approximation. The panels in blue background (a), (b) are the results for our scheme. The panels in yellow background (c), (d) are the results when the system is coupled to thermal baths. All the results are averaged over 100 trajectories with different disorder configurations. Parameters are $U = 0$, $\gamma = 0.01J$, $\lambda_L = 0.1$, $\lambda_R = 1$, $T_L = 10J$, and $T_R = 0.01J$.

the non-interacting system becomes apparent from the saturation of the heat current. While it would have been interesting to study numerically, whether/how ballistic transport breaks down with increasing interactions, we would like to point out that our scheme opens the opportunity to investigate this question experimentally in a quantum simulation, where heat-current-carrying states also of larger interacting systems are prepared using feedback control.

4.4. Influence of disorder

Here we investigate the influence of disorder on the steady-state heat current. For this purpose, we add a random on-site potential, with V_l being a random number uniformly distributed in the range $[-V_d, V_d]$. The results are shown in figure 6, which are averaged over 100 trajectories with different disorder configurations. From figure 6(a) one can see that the current decreases exponentially with the disorder strength V_d. Such a behavior is expected as a result of Anderson localization [57], which describes the suppression of transport (i.e. wave propagation) in a system with disordered potential due to dephasing upon scattering events from randomly-distributed impurities. Figure 6(b) shows the current as a function of the lattice site number M at $V_d = 0.2J$ and fixed filling $N/M = 1/5$. The decay of the current with increasing system size is approximately exponential, as indicated by the close-to-linear form of the current in the log-y plot. Similar behaviors are observed when the system is coupled to real thermal baths, as shown in figures 6(c) and (d).

5. Experimental implementation

Now we discuss the experimental implementation of our scheme. For the engineering of the local baths, one needs to perform measurements of the on-site population, and add the corresponding feedback control. The

former can be implemented via homodyne detection of the off-resonant scattering of structured probe light from the atoms [58–60]. To engineer two independent baths, one can for instance use two probe beams with different frequencies. The feedback control of tunneling with complex rate can be realized by modulating the on-site energy of the relevant sites (see appendix C).

For the heat current, we propose to make use of the measurement of single-particle density matrices $\langle a_i^\dagger a_j\rangle$, which is experimentally accessible [61]. It can be shown that the heat current is given by

$$\begin{aligned}\frac{\mathcal{J}_L}{\gamma} =& \frac{J}{2}[(x+x^{-1})^2+4\lambda_L^2]\langle a_1^\dagger a_2+a_2^\dagger a_1\rangle+\frac{J}{2}(\lambda_L^2+x^{-2})\langle a_2^\dagger a_3+a_3^\dagger a_2\rangle\\ &+J\lambda_L(x+x^{-1})\langle(a_1^\dagger a_2-a_2^\dagger a_1)^2\rangle-2J\lambda_L\langle(n_1-n_2)(xn_1-x^{-1}n_2)\rangle\\ &-\frac{J\lambda_L}{2}\langle(a_1^\dagger a_3+a_3^\dagger a_1)(xn_1-x^{-1}n_2)+\text{h.c.}\rangle\\ &-\frac{J\lambda_L}{2x}\langle(a_1^\dagger a_2-a_2^\dagger a_1)(a_2^\dagger a_3-a_3^\dagger a_2)+\text{h.c.}\rangle\\ &-\frac{U\lambda_L}{4}\langle(xn_1-x^{-1}n_2)(n_1-n_2)(a_1^\dagger a_2+a_2^\dagger a_1)+\text{h.c.}\rangle\\ &-\frac{U\lambda_L}{4}\langle(n_1-n_2)(a_1^\dagger a_2+a_2^\dagger a_1)(xn_1-x^{-1}n_2)+\text{h.c.}\rangle\\ &-U\lambda_L^2(\langle(n_1-n_2)^2\rangle-\langle(a_1^\dagger a_2+a_2^\dagger a_1)^2\rangle),\end{aligned} \tag{20}$$

with $x=x_1=g_2/g_1$. By using Wick's theorem, corresponding to the mean-field approximation used already for the kinetic theory,

$$\langle a_k^\dagger a_q a_p^\dagger a_l\rangle\approx\langle a_k^\dagger a_q\rangle\langle a_p^\dagger a_l\rangle+\langle a_k^\dagger a_l\rangle\langle a_q a_p^\dagger\rangle,$$

we have

$$\langle(a_1^\dagger a_2-a_2^\dagger a_1)^2\rangle\approx\langle a_1^\dagger a_2-a_2^\dagger a_1\rangle^2+\langle a_1^\dagger a_2\rangle^2+\langle a_2^\dagger a_1\rangle^2-2\langle n_1\rangle\langle n_2\rangle-\langle n_1\rangle-\langle n_2\rangle, \tag{21}$$

$$\langle(n_1-n_2)(xn_1-x^{-1}n_2)\rangle\approx x\langle n_1\rangle(2\langle n_1\rangle-\langle n_2\rangle+1)+x^{-1}\langle n_2\rangle(2\langle n_2\rangle-\langle n_1\rangle+1)-(x+x^{-1})|\langle a_1^\dagger a_2\rangle|^2, \tag{22}$$

$$\begin{aligned}&\langle(a_1^\dagger a_3+a_3^\dagger a_1)(xn_1-x^{-1}n_2)+\text{h.c.}\rangle\approx\langle a_1^\dagger a_3+a_3^\dagger a_1\rangle(4x\langle n_1\rangle-2x^{-1}\langle n_2\rangle+x)\\ &\quad-4x^{-1}\text{Re}(\langle a_1^\dagger a_2\rangle\langle a_2^\dagger a_3\rangle),\end{aligned} \tag{23}$$

$$\begin{aligned}&\langle(a_1^\dagger a_2-a_2^\dagger a_1)(a_2^\dagger a_3-a_3^\dagger a_2)+\text{h.c.}\rangle\\ &\quad\approx 2\langle a_1^\dagger a_2-a_2^\dagger a_1\rangle\langle a_2^\dagger a_3-a_3^\dagger a_2\rangle+\langle a_1^\dagger a_3+a_3^\dagger a_1\rangle(2\langle n_2\rangle+1)-4\text{Re}(\langle a_1^\dagger a_2\rangle\langle a_3^\dagger a_2\rangle),\end{aligned} \tag{24}$$

$$\langle(n_1-n_2)^2\rangle-\langle(a_1^\dagger a_2+a_2^\dagger a_1)^2\rangle\approx 2\langle n_1-n_2\rangle^2-4\text{Re}(\langle a_1^\dagger a_2\rangle^2)-4|\langle a_1^\dagger a_2\rangle|^2, \tag{25}$$

$$\begin{aligned}&\langle(xn_1-x^{-1}n_2)(n_1-n_2)(a_1^\dagger a_2+a_2^\dagger a_1)+(n_1-n_2)(a_1^\dagger a_2+a_2^\dagger a_1)(xn_1-x^{-1}n_2)+\text{h.c.}\rangle\\ &\approx 4\langle a_1^\dagger a_2+a_2^\dagger a_1\rangle\left\{x\left[6\langle n_1\rangle^2+4\langle n_1\rangle\right]+x^{-1}\left[6\langle n_2\rangle^2+4\langle n_2\rangle\right]\right.\\ &\quad\left.-(x+x^{-1})[4\langle n_1\rangle\langle n_2\rangle+\langle n_1\rangle+\langle n_2\rangle+2|\langle a_1^\dagger a_2\rangle|^2]\right\}.\end{aligned} \tag{26}$$

A comparison between the exact results of the individual terms and the mean-field approximation is presented in appendix D. In figure 7, we compare the exact results of the steady-state heat current and the approximated ones by using equations (21)–(24). Note that for the latter, we neglect the interaction terms proportional to U in equation (20) since they are small and cannot be expected to be captured within mean-field theory (see appendix D for details). For the non-interacting case (see the blue data in figure 7(a)), the approximation is found to be very good, especially for λ_L close to 0 or 1. For the interacting case (see the orange data in figure 7(a) and the results in figure 7(b)), the approximated results still capture the behavior very well. These results confirm the feasibility to measure the heat current for our scheme in experiments.

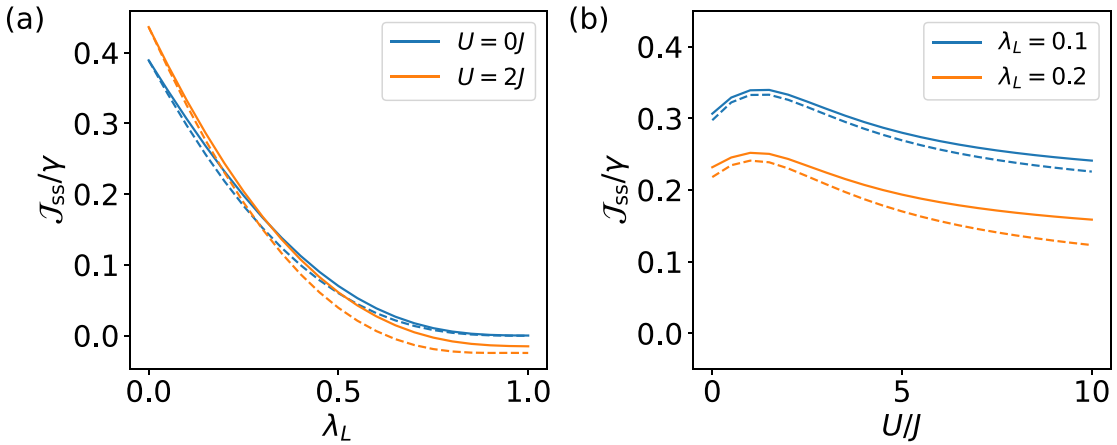

Figure 7. The steady-state heat current $\mathcal{J}_{ss}$ as a function of (a) the feedback strength λ_L for two different interaction strengths U, and (b) the interaction strength U for two different feedback strength λ_L. Parameters are $N = 2$, $M = 10$, $V_l = 0$, $\gamma = 0.01J$, and $\lambda_R = 1$. The solid lines are exact results. The dashed lines are the approximated results by using Wick's decomposition, equations (21)–(24).

6. Conclusion

In conclusion, we have proposed a scheme for the realization of heat-current-carrying states of ultracold atoms in an optical lattice using Markovian feedback control. Measurements and feedback control are implemented at the boundaries of the lattice to mimic the effect of coupling the system locally to two thermal baths with different temperature. We studied the scaling of the steady-state heat current with system size by using two approaches: semi-classical MC simulation and kinetic theory. For the non-interacting case, both approaches show good agreement with the results from ED (accessible for small systems). When the particle number is fixed, the current decays with the lattice size as M^{-1}. For a fixed filling factor, the current is found to decay at first, but rapidly saturate at a finite value, independent of the system size. Namely, the system exhibits ballistic transport. For the interacting systems with a fixed filling factor, our simulations are restricted to rather small system sizes, so that it is hard to investigate, how ballistic transport is modified or destroyed as a result of interactions. However, our scheme opens a door towards the experimental investigation of this problem in a quantum simulator of ultracold atoms. In the presence of disorder, the current for a system with a fixed filling factor is found to decay exponentially with the system size. These results confirm that the heat current generated by the feedback-engineered baths shows the same scaling behavior as those resulting from actual thermal baths. We also discussed the experimental implementation of our scheme and, in particular, described how the heat current can be measured in the laboratory. Our findings can be tested by available experimental techniques. Our approach opens a new path for the experimental investigation of heat-current-carrying states of large interacting systems for which a theoretical prediction is challenging. Thus it offers a new route for the quantum simulation of transport phenomena with ultracold atoms.

Data availability statement

The data that support the findings of this study are available upon reasonable request from the authors.

Acknowledgement

This research was funded by the German Research Foundation (DFG) within the collaborative research center (SFB) 910 under project number 163436311.

Appendix A

Here we analyze the heat current in our feedback scheme for a single-particle problem. In this case, the mean occupations in the eigenstates for the steady state satisfy

$$\sum_q \left[R_{kq}\langle n_q\rangle_{ss} - R_{qk}\langle n_k\rangle_{ss}\right] = 0, \tag{A.1}$$

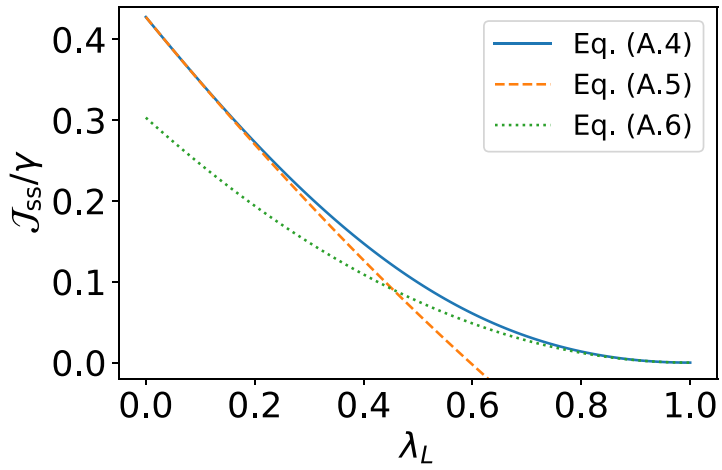

Figure A1. The steady-state heat current $\mathcal{J}_{ss}$ as a function of the feedback strength λ_L. Parameters are $N=1$, $M=5$, $V_l=0$, $\gamma=0.01J$, and $\lambda_R=1$. The solid line is the exact result given by equation (A.4). The dashed line is the approximated result equation (A.5) for $\lambda_L\simeq 0$. The dotted line is the approximated result equation (A.6) for $\lambda_L\simeq 1$.

where the single-particle transfer rate $R_{kq}=R^L_{kq}+R^R_{kq}$ with

$$\begin{aligned} R^L_{kq} &= \gamma\left(\frac{2}{M+1}\right)^2\left[\frac{\sin(\alpha)}{\sin(2\alpha)}\sin(k\alpha)\sin(q\alpha)-\frac{\sin(2\alpha)}{\sin(\alpha)}\sin(2k\alpha)\sin(2q\alpha)\right.\\ &\quad\left.-\lambda_L\sin(k\alpha)\sin(2q\alpha)+\lambda_L\sin(2k\alpha)\sin(q\alpha)\right]^2,\\ R^R_{kq} &= \gamma\left(\frac{2}{M+1}\right)^2\left[\frac{\sin(2\alpha)}{\sin(3\alpha)}\sin(3k\alpha)\sin(3q\alpha)-\frac{\sin(3\alpha)}{\sin(2\alpha)}\sin(2k\alpha)\sin(2q\alpha)\right.\\ &\quad\left.-\lambda_R\sin(3k\alpha)\sin(2q\alpha)+\lambda_R\sin(2k\alpha)\sin(3q\alpha)\right]^2, \end{aligned} \tag{A.2}$$

with $\alpha=\pi/(M+1)$. By solving equation (A.1), one gets the steady-state mean occupation $\langle n_k\rangle_{ss}$. The steady-state heat current is then given by

$$\mathcal{J}_{ss}=-\sum_k\epsilon_k\sum_q\left[R^L_{kq}\langle n_q\rangle_{ss}-R^L_{qk}\langle n_k\rangle_{ss}\right]. \tag{A.3}$$

Here we show an example to demonstrate the dependence of heat current on the control parameter λ_L with $\lambda_R=1$. For $M=5$, the heat current reads

$$\mathcal{J}_{ss}/\gamma=\frac{2940\lambda_L^8-6400\lambda_L^7+16904\lambda_L^6-35856\lambda_L^5+64852\lambda_L^4-111104\lambda_L^3+183000\lambda_L^2-192960\lambda_L+78624}{\sqrt{3}(1050\lambda_L^8+10195\lambda_L^6-7680\sqrt{3}\lambda_L^5+41178\lambda_L^4-34032\lambda_L^3+94923\lambda_L^2-56160\lambda_L+106110)}. \tag{A.4}$$

For $\lambda_L\simeq 0$, it can be approximated by

$$\mathcal{J}_{ss}/\gamma\simeq\frac{155225108\lambda_L^2}{505820475\sqrt{3}}-\frac{1101472\lambda_L}{772245\sqrt{3}}+\frac{1456}{1965\sqrt{3}}. \tag{A.5}$$

For $\lambda_L\simeq 1$, equation (A.4) can be approximated by

$$\mathcal{J}_{ss}/\gamma\simeq\frac{3405\sqrt{3}(1-\lambda_L)^2}{19448}. \tag{A.6}$$

Figure A1 compares these results.

Appendix B

Here we describe the calculation of heat transport when the system is coupled to thermal baths.

The coupling of the system to thermal baths induces quantum jumps between the eigenstates of the system [56]. When the system is coupled at its boundaries to two thermal baths with different

temperatures (see the sketch in figure 3 of the main text), the dynamics of the system is described by the following ME,

$$\dot{\rho} = -i[H,\rho] + \mathcal{L}_L\rho + \mathcal{L}_R\rho, \tag{B.1}$$

with

$$\mathcal{L}_\mu\rho = \sum_{k,q}\left(L_{kq}^{(\mu)}\rho L_{kq}^{(\mu)\dagger} - \frac{1}{2}\left\{L_{kq}^{(\mu)\dagger}L_{kq}^{(\mu)},\rho\right\}\right), \quad \mu = L,R. \tag{B.2}$$

Here the jump operators

$$L_{kq}^{(\mu)} = \sqrt{R_{kq}^{\mu}}|k\rangle\langle q| \tag{B.3}$$

describe the quantum jump from eigenstate $|q\rangle$ to $|k\rangle$ with the jump rates

$$R_{kq}^{\mu} = 2\pi\gamma\nu_{kq}^{\mu}g_\mu(E_k - E_q), \tag{B.4}$$

where the coupling matrix element is given by

$$\begin{aligned}\nu_{kq}^{L} &= |\langle k|n_1|q\rangle|^2 + |\langle k|n_2|q\rangle|^2,\\ \nu_{kq}^{R} &= |\langle k|n_{M-2}|q\rangle|^2 + |\langle k|n_{M-1}|q\rangle|^2,\end{aligned} \tag{B.5}$$

and bath correlation function

$$g_\mu(E) = \frac{E}{e^{E/(k_BT_\mu)}-1}. \tag{B.6}$$

The steady state is calculated by solving $\dot{\rho} = 0$, and the heat current is then obtained by calculating equation (12) in the main text. For the kinetic theory, similar calculations are performed as for the feedback scheme, just with the rates R_{kq}^{μ} replaced by equation (B.4) for the thermal baths.

Appendix C

Here we discuss the implementation of the feedback control terms. By including the feedback terms to the Hamiltonian, we arrive at

$$H'(t) = -(J_L(t)a_1^\dagger a_2 + J_R(t)a_{M-2}^\dagger a_{M-1} + J\sum_{l\neq 1,M-2}a_l^\dagger a_{l+1} + \text{h.c.}) + H_U + H_V, \tag{C.1}$$

where H_U and H_V denote the original interaction and on-site potential terms in (1) and

$$J_\mu(t) = J + i\sqrt{\gamma}\lambda_\mu I_{\text{hom}}(t) = \sqrt{J^2+\gamma\lambda_\mu^2 I_{\text{hom}}^2}e^{i\theta_\mu(t)}, \quad \mu = L,R, \tag{C.2}$$

with $\tan\theta_\mu = \sqrt{\gamma}\lambda_\mu I_{\text{hom}}/J$. Our goal is to implement such a Hamiltonian.

We can achieve it by modulating the on-site energy of the relevant sites so that the system Hamiltonian reads

$$H_d(t) = -\sum_{l=1}^{M-1}(J_l a_l^\dagger a_{l+1} + \text{h.c.}) + H_U + H_V + \Delta_L(t)n_1 - \Delta_R(t)(n_{M-1}+n_M). \tag{C.3}$$

In the rotating frame with transformation $U(t) = \exp\{i\int[\Delta_L(t_1)n_1 - \Delta_R(t_1)(n_{M-1}+n_M)]dt_1\}$, the Hamiltonian is given by

$$\begin{aligned}\tilde{H}_d(t) &= UHU^\dagger + i\dot{U}U^\dagger\\ &= -(J_1e^{i\theta_L(t)}a_1^\dagger a_2 + J_{M-2}e^{i\theta_R(t)}a_{M-2}^\dagger a_{M-1} + \sum_{l\neq 1,M-2}J_l a_l^\dagger a_{l+1} + \text{h.c.}) + H_U + H_V,\end{aligned} \tag{C.4}$$

with $\theta_\mu(t) = \int\Delta_\mu(t_1)dt_1$. By comparing equations (C.1) and (C.4), one can read off

$$J_1 = \sqrt{J^2+\gamma\lambda_L^2 I_{\text{hom}}^2}, J_{M-2} = \sqrt{J^2+\gamma\lambda_R^2 I_{\text{hom}}^2}, \int\Delta_\mu(t_1)dt_1 = \arctan(\sqrt{\gamma}\lambda_\mu I_{\text{hom}}/J), \tag{C.5}$$

and $J_l = J$ for $l \neq 1, M-2$.

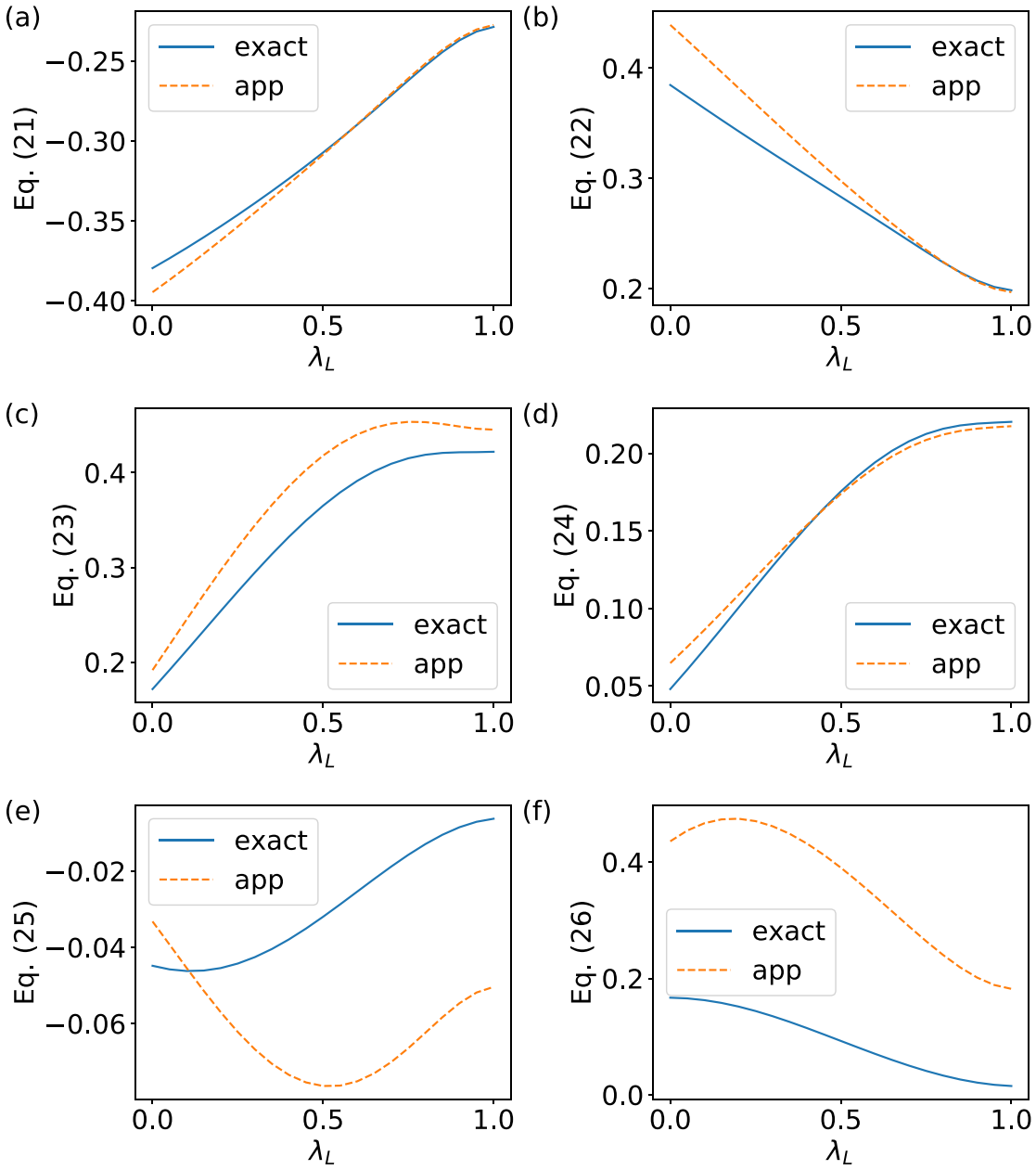

Figure D1. Checking equations (21)–(26) in the main text. The solid (dashed) lines denote the results of the left (right) hand side of these equations. The parameters are $N = 2$, $M = 10$, $U = 2J$, $V_l = 0$, $\gamma = 0.01J$, and $\lambda_R = 1$.

Appendix D

Here we check the validity of equations (21)–(26) in the main text. Figure D1 compares the left (solid lines) and right (dashed lines) hand side of these terms. One can see that for the terms relevant for tunneling effects, i.e. (a)–(d), the approximations are good. They become worse when it comes to the terms relevant to interactions, i.e. (e)–(f). The worse performance of the approximation in (f) is attributed to the involved higher order correlations compared with other terms. Due to the bad performance of the approximation in the two interaction-relevant terms, we neglect them in the calculation of the approximated heat current. Note that the term in (e) has very small value, and thus its influence is small. For the term in (f), from the expression of the heat current, equation (20) in the main text, one can see that it is proportional to λ_L^2, and thus its effect is weak for small λ_L. This observation is in consistent with the results shown in figure 7 of the main text.

ORCID iDs

Ling-Na Wu https://orcid.org/0000-0003-4722-5883
André Eckardt https://orcid.org/0000-0002-5542-3516

References

[1] Bloch I, Dalibard J and Zwerger W 2008 Many-body physics with ultracold gases *Rev. Mod. Phys.* **80** 885–964
[2] Bertini B, Heidrich-Meisner F, Karrasch C, Prosen T, Steinigeweg R and Žnidarič M 2021 Finite-temperature transport in one-dimensional quantum lattice models *Rev. Mod. Phys.* **93** 025003
[3] Landi G T, Poletti D and Schaller G 2021 Non-equilibrium boundary driven quantum systems: models, methods and properties (arXiv:2104.14350)
[4] Anderson R, Wang F, Xu P, Venu V, Trotzky S, Chevy Féric and Thywissen J H 2019 Conductivity spectrum of ultracold atoms in an optical lattice *Phys. Rev. Lett.* **122** 153602
[5] Brown P T *et al* 2019 Bad metallic transport in a cold atom Fermi-Hubbard system *Science* **363** 379–82
[6] Pasienski M, McKay D, White M and DeMarco B 2010 A disordered insulator in an optical lattice *Nat. Phys.* **6** 677–80
[7] Kondov S S, McGehee W R, Xu W and DeMarco B 2015 Disorder-induced localization in a strongly correlated atomic Hubbard gas *Phys. Rev. Lett.* **114** 083002
[8] Ott H, de Mirandes E, Ferlaino F, Roati G, Modugno G and Inguscio M 2004 Collisionally induced transport in periodic potentials *Phys. Rev. Lett.* **92** 160601
[9] Pezzè L, Pitaevskii L, Smerzi A, Stringari S, Modugno G, de Mirandes E, Ferlaino F, Ott H, Roati G and Inguscio M 2004 Insulating behavior of a trapped ideal Fermi gas *Phys. Rev. Lett.* **93** 120401
[10] Fertig C D, O'Hara K M, Huckans J H, Rolston S L, Phillips W D and Porto J V 2005 Strongly inhibited transport of a degenerate 1D Bose gas in a lattice *Phys. Rev. Lett.* **94** 120403
[11] Strohmaier N, Takasu Y, Günter K, Jördens R, Köhl M, Moritz H and Esslinger T 2007 Interaction-controlled transport of an ultracold Fermi gas *Phys. Rev. Lett.* **99** 220601
[12] Clément D, Varón A F, Hugbart M, Retter J A, Bouyer P, Sanchez-Palencia L, Gangardt D M, Shlyapnikov G V and Aspect A 2005 Suppression of transport of an interacting elongated Bose–Einstein condensate in a random potential *Phys. Rev. Lett.* **95** 170409
[13] Fort C, Fallani L, Guarrera V, Lye J E, Modugno M, Wiersma D S and Inguscio M 2005 Effect of optical disorder and single defects on the expansion of a Bose–Einstein condensate in a one-dimensional waveguide *Phys. Rev. Lett.* **95** 170410
[14] Robert-de-Saint-Vincent M, Brantut J-P, Allard B, Plisson T, Pezzé L, Sanchez-Palencia L, Aspect A, Bourdel T and Bouyer P 2010 Anisotropic 2D diffusive expansion of ultracold atoms in a disordered potential *Phys. Rev. Lett.* **104** 220602
[15] Roati G, D'Errico C, Fallani L, Fattori M, Fort C, Zaccanti M, Modugno G, Modugno M and Inguscio M 2008 Anderson localization of a non-interacting Bose–Eeinstein condensate *Nature* **453** 895–8
[16] Billy J *et al* 2008 Direct observation of Anderson localization of matter waves in a controlled disorder *Nature* **453** 891–4
[17] Deissler B, Zaccanti M, Roati G, D'Errico C, Fattori M, Modugno M, Modugno G and Inguscio M 2010 Delocalization of a disordered bosonic system by repulsive interactions *Nat. Phys.* **6** 354–8
[18] Kondov S S, McGehee W R, Zirbel J J and DeMarco B 2011 Three-dimensional Anderson localization of ultracold matter *Science* **334** 66–68
[19] Jendrzejewski F, Bernard A, Müller K, Cheinet P, Josse V, Piraud M, Pezzé L, Sanchez-Palencia L, Aspect A and Bouyer P 2012 Three-dimensional localization of ultracold atoms in an optical disordered potential *Nat. Phys.* **8** 398–403
[20] Choi J-Y, Hild S, Zeiher J, Schauß P, Rubio-Abadal A, Yefsah T, Khemani V, Huse D A, Bloch I and Gross C 2016 Exploring the many-body localization transition in two dimensions *Science* **352** 1547–52
[21] Ronzheimer J P, Schreiber M, Braun S, Hodgman S S, Langer S, McCulloch I P, Heidrich-Meisner F, Bloch I and Schneider U 2013 Expansion dynamics of interacting bosons in homogeneous lattices in one and two dimensions *Phys. Rev. Lett.* **110** 205301
[22] Schneider U *et al* 2012 Fermionic transport and out-of-equilibrium dynamics in a homogeneous Hubbard model with ultracold atoms *Nat. Phys.* **8** 213–8
[23] Krinner S, Stadler D, Husmann D, Brantut J-P and Esslinger T 2015 Observation of quantized conductance in neutral matter *Nature* **517** 64–67
[24] Krinner S, Lebrat M, Husmann D, Grenier C, Brantut J-P and Esslinger T 2016 Mapping out spin and particle conductances in a quantum point contact *Proc. Natl Acad. Sci.* 113 8144–9
[25] Krinner S, Esslinger T and Brantut J-P 2017 Two-terminal transport measurements with cold atoms *J. Phys.: Condens. Matter.* **29** 343003
[26] Lebrat M, Grišins P, Husmann D, Häusler S, Corman L, Giamarchi T, Brantut J-P and Esslinger T 2018 Band and correlated insulators of cold fermions in a mesoscopic lattice *Phys. Rev.* X **8** 011053
[27] Sommer A, Ku M, Roati G and Zwierlein M W 2011 Universal spin transport in a strongly interacting Fermi gas *Nature* **472** 201–4
[28] Fukuhara T *et al* 2013 Quantum dynamics of a mobile spin impurity *Nat. Phys.* **9** 235–41
[29] Valtolina G, Scazza F, Amico A, Burchianti A, Recati A, Enss T, Inguscio M, Zaccanti M and Roati G 2017 Exploring the ferromagnetic behaviour of a repulsive Fermi gas through spin dynamics *Nat. Phys.* **13** 704–9
[30] Nichols M A, Cheuk L W, Okan M, Hartke T R, Mendez E, Senthil T, Khatami E, Zhang H and Zwierlein M W 2019 Spin transport in a Mott insulator of ultracold fermions *Science* **363** 383–7
[31] Koschorreck M, Pertot D, Vogt E and Köhl M 2013 Universal spin dynamics in two-dimensional Fermi gases *Nat. Phys.* **9** 405–9
[32] Hild S, Fukuhara T, Schauß P, Zeiher J, Knap M, Demler E, Bloch I and Gross C 2014 Far-from-equilibrium spin transport in Heisenberg quantum magnets *Phys. Rev. Lett.* **113** 147205
[33] Luciuk C, Smale S, Böttcher F, Sharum H, Olsen B A, Trotzky S, Enss T and Thywissen J H 2017 Observation of quantum-limited spin transport in strongly interacting two-dimensional Fermi gases *Phys. Rev. Lett.* **118** 130405
[34] Bardon A B *et al* 2014 Transverse demagnetization dynamics of a unitary Fermi gas *Science* **344** 722–4
[35] Trotzky S, Beattie S, Luciuk C, Smale S, Bardon A B, Enss T, Taylor E, Zhang S and Thywissen J H 2015 Observation of the Leggett-Rice effect in a unitary Fermi gas *Phys. Rev. Lett.* **114** 015301
[36] Jepsen P N, Amato-Grill J, Dimitrova I, Ho W W, Demler E and Ketterle W 2020 Spin transport in a tunable Heisenberg model realized with ultracold atoms *Nature* **588** 403–7

[37] Meppelink R, van Rooij R, Vogels J M and van der Straten P 2009 Enhanced heat flow in the hydrodynamic collisionless regime *Phys. Rev. Lett.* **103** 095301
[38] Brantut J-P, Grenier C, Meineke J, Stadler D, Krinner S, Kollath C, Esslinger T and Georges A 2013 A thermoelectric heat engine with ultracold atoms *Science* **342** 713–5
[39] Häusler S, Fabritius P, Mohan J, Lebrat M, Corman L and Esslinger T 2021 Interaction-assisted reversal of thermopower with ultracold atoms *Phys. Rev.* X **11** 021034
[40] Wiseman H M 1994 Quantum theory of continuous feedback *Phys. Rev.* A **49** 2133–50
[41] Wang J and Wiseman H M 2001 Feedback-stabilization of an arbitrary pure state of a two-level atom *Phys. Rev.* A **64** 063810
[42] Campagne-Ibarcq P, Jezouin S, Cottet N, Six P, Bretheau L, Mallet F, Sarlette A, Rouchon P and Huard B 2016 Using spontaneous emission of a qubit as a resource for feedback control *Phys. Rev. Lett.* **117** 060502
[43] Wang J, Wiseman H M and Milburn G J 2005 Dynamical creation of entanglement by homodyne-mediated feedback *Phys. Rev.* A **71** 042309
[44] Carvalho A R R and Hope J J 2007 Stabilizing entanglement by quantum-jump-based feedback *Phys. Rev.* A **76** 010301
[45] Carvalho A R R, Reid A J S and Hope J J 2008 Controlling entanglement by direct quantum feedback *Phys. Rev.* A **78** 012334
[46] Wang L C, Shen J and Yi X X 2010 Effect of feedback control on the entanglement evolution *Eur. Phys. J.* D **56** 435–40
[47] Tombesi P and Vitali D 1994 Physical realization of an environment with squeezed quantum fluctuations via quantum-nondemolition-mediated feedback *Phys. Rev.* A **50** 4253–7
[48] Thomsen L K, Mancini S and Wiseman H M 2002 Spin squeezing via quantum feedback *Phys. Rev.* A **65** 061801
[49] Buonaiuto G, Carollo F, Olmos B and Lesanovsky I 2021 Dynamical phases and quantum correlations in an emitter-waveguide system with feedback *Phys. Rev. Lett.* **127** 133601
[50] Wu L-N and Eckardt A 2022 Cooling and state preparation in an optical lattice via Markovian feedback control *Phys. Rev. Res.* **4** L022045
[51] Wu L-N and Eckardt A 2022 Quantum engineering of a synthetic thermal bath for bosonic atoms in a one-dimensional optical lattice via markovian feedback control *SciPost Phys.* **13** 059
[52] Wiseman H M and Milburn G J 2009 *Quantum Measurement and Control* (Cambridge: Cambridge University Press)
[53] Vorberg D, Wustmann W, Schomerus H, Ketzmerick R and Eckardt A 2015 Nonequilibrium steady states of ideal bosonic and fermionic quantum gases *Phys. Rev.* E **92** 062119
[54] Breuer H P and Petruccione F 2002 *The Theory of Open Quantum Systems* (Oxford: Oxford University Press)
[55] Dalibard J, Castin Y and Mølmer K 1992 Wave-function approach to dissipative processes in quantum optics *Phys. Rev. Lett.* **68** 580–3
[56] Daley A J 2014 Quantum trajectories and open many-body quantum systems *Adv. Phys.* **63** 77–149
[57] Anderson P W 1958 Absence of diffusion in certain random lattices *Phys. Rev.* **109** 1492–505
[58] Elliott T J, Kozlowski W, Caballero-Benitez S F and Mekhov I B 2015 Multipartite entangled spatial modes of ultracold atoms generated and controlled by quantum measurement *Phys. Rev. Lett.* **114** 113604
[59] Ashida Y and Ueda M 2015 Diffraction-unlimited position measurement of ultracold atoms in an optical lattice *Phys. Rev. Lett.* **115** 095301
[60] Ritsch H, Domokos P, Brennecke F and Esslinger T 2013 Cold atoms in cavity-generated dynamical optical potentials *Rev. Mod. Phys.* **85** 553–601
[61] Pe\ña Ardila L A, Heyl M and Eckardt A 2018 Measuring the single-particle density matrix for fermions and hard-core bosons in an optical lattice *Phys. Rev. Lett.* **121** 260401